Journal of Intelligent & Robotic Systems (2022) 106: 31
https://doi.org/10.1007/s10846-022-01738-6

SHORT PAPER

Research on Robotic Humanoid Venipuncture Method Based on Biomechanical Model

Tianbao He[1] · Chuangqiang Guo[1] · Hansong Liu[1] · Li Jiang[1]

Received: 6 February 2022 / Accepted: 28 August 2022 / Published online: 17 September 2022

Abstract
Automatic venipuncture robots are expected to replace manual venipuncture methods owing to their high control precision, steady operation, and measurable perception. However, the lack of perception of the venipuncture status in the human body leads to an increased risk and failure rate, which further restricts the development of such robots. To address this, we propose a humanoid venipuncture method guided by a biomechanical model to imitate human sensations and feedback. This method intends to perceive the venipuncture status and improve the performance of the venipuncture robot. First, this study establishes a biomechanical venipuncture model, which thoroughly considers the elastic deformation, cutting, and friction of tissues and can be applied to different venipuncture conditions. Then, venipuncture simulations and in vitro phantom experiments are performed under various settings to analyze and validate the model. Finally, to evaluate the robotic humanoid venipuncture method, we apply the method to a self-developed six-degree-of-freedom venipuncture robot via rabbit ear veins with a success rate of approximately 90%. This work demonstrates that the humanoid venipuncture method based on the biomechanical model is practical and rapid in processing simple information in venipuncture robots.

Keywords Biomechanical model · Force feedback · Status perception · Venipuncture robot

1 Introduction

Venipuncture is obtaining a blood sample or applying an injection of medication by puncturing a vein. Manual venipuncture is currently the primary method used. Statistics show that the total number of venipunctures performed worldwide is approximately 3.5 million per day [1], with about 85 percent of medical staff spending more than 75 percent of their time on the procedure [2]. It is evident that manual venipuncture consumes massive amounts of healthcare resources; therefore, it is of great social importance to liberate healthcare resources from venipuncture tasks.

Numerous medical problems have been solved with the evolution of medical robot technology. For example, the da Vinci surgical robot [3] and the puncture robot [4] have the features of high motion precision, robust perceptual performance, powerful data processing, and excellent stability because of their intelligent control method and creative mechanism design [5–8]. Moreover, the spread of covid-19 raises new challenges for protecting medical staff. Using robots to assist in medical procedures enhances accuracy and efficiency and minimizes the risk of medical staff getting the virus. Under the remote operation of medical staff, the robot's motion error was within an acceptable range of 5mm during minimally invasive surgeries [9], and a success rate of 95 percent could be reached when collecting oropharyngeal swabs samples for covid-19 [10].

Consequently, venipuncture robots are anticipated to undertake venipuncture to alleviate the burden on medical staff and reduce cross-infection when COVID-19 is raging. Regarding mechanism design, the venipuncture robots have advanced from single to multiple degree-of-freedom designs [7–13], which allow for more flexible motions with multiple angles of the puncture needle. Further, the needle can be controlled effectively to reach the target site with excellent vein recognition. However, the lack of in vivo puncture state sensing (current depth and position) limits effective control of the needle entering the target vein stably, making these robots less successful and more risky. Therefore, enabling venipuncture robots to sense the puncture states is an urgent research problem that must be solved.

✉ Li Jiang
jiangli01@hit.edu.cn

[1] State Key Laboratory of Robotics and System, Harbin Institute of Technology, Harbin 150001, China

Currently, the leading solution to this problem is to use ultrasound equipment to observe the puncture process in real-time [11–13]. However, ultrasound imaging depends on the tissue cross-section, so it is vital to ensure that the needle and veins are always located within the field of ultrasound imaging during the puncture [5, 11]. Once the needle is not aligned with the imaging cross-section of the ultrasound device during its movement, the needle falls into an observation blind spot, increasing the risk of puncture failure. Moreover, ultrasound imaging has a lengthy learning time [14, 15], and image processing is complicated [16, 17]. Studies have also been reported on the electrical impedance of biological tissues. As the electrical impedance of blood is lower than in other tissues [18–21], changes in the electrical impedances during puncture are detected to determine whether the puncture needle enters the vessel [22–24]. Although this method is simple and low cost, it requires modification of the needle to detect electrical impedances, which cause blood contamination and potential harm. Therefore, these two methods cannot solve the puncture state sensing problem.

We note that the human hand, aided by the central nervous system, is capable of various fine manipulative movements [25, 26], so more research focuses on humanoid behavior and anthropomorphic control methods [27, 28]. Manual venipuncture is mainly dependent on touch-pressure sensations and the nervous system. In manual venipuncture (Fig. 1), changes in the force on the needle perceived by the human hand are transmitted to the brain via sensory nerves. The sensory centers in the cerebral cortex process these signals. Once the puncture needle enters the vessel, the movement of the needle becomes smoother owing to changes in the puncture force. When the haptic center senses this change, the brain senses that the needle has entered the vein and commands the hand muscles to stop. The introduction of force control in robotic systems has been widely proved feasible and effective for improving control performance [29–31]. Consequently, if venipuncture robots can be equipped with humanoid force perception, the inability to perceive the in vivo puncture status is expected to be solved.

We attempt to establish a biomechanical model of venipuncture by exploring the changing patterns and influencing factors of puncture forces. The model is able to guide the robot to imitate human sensations and feedback to assess status and position during automatic venipuncture. Some scholars have already studied the puncture processes in biological tissues and established the corresponding biomechanical models. For example, Jiang et al. [32] experimentally analyzed the relationship between the interaction force between needle and tissue, the shape of the needle tip, and the diameter of the needle. They concluded that the insertion force was more significant in skin and muscle than fat. Barnett et al. [33] measured the fracture toughness, friction, and

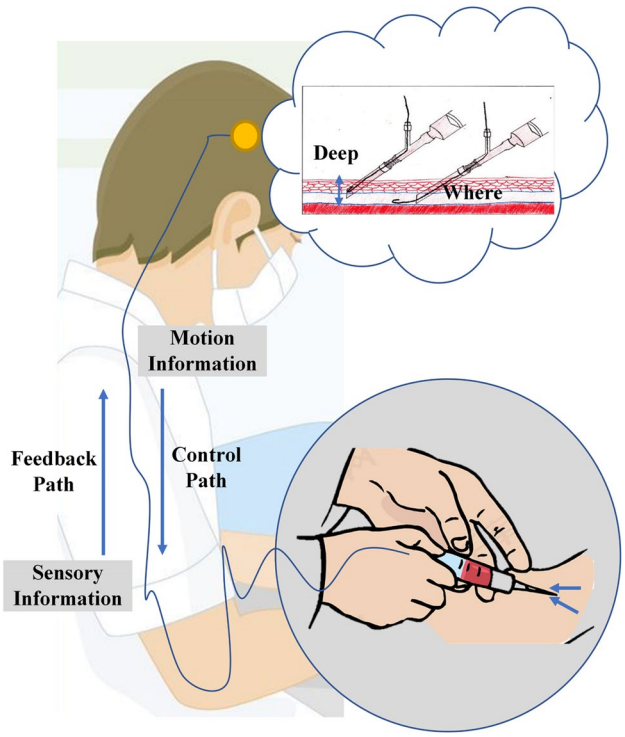

Fig. 1 Perception and manipulation in manual venipuncture

crack length using different needle sizes and insertion speeds on a puncture phantom and concluded that the increase in insertion speed could not reduce the insertion force.

Okamura et al. [34] and Fischer et al. [35] studied and modeled the forces of puncturing bovine liver and prostate, respectively. Su [36] studied a complete puncture force model in pig viscera, including the effects of needle insertion speed, angle, and tip shape on puncture force. However, unlike organ cutting, venipuncture cuts through multiple layers of tissue and then enters the vessel, thereby excluding these biomechanical models. Moreover, standardized disposable puncture needles with a consistent tip shape and diameter are used during venipuncture, eliminating the influence of different needles. Other scholars have conducted studies and biomechanical modeling for the puncture of flexible needles [32, 37–39]. The puncture force modeling in such studies needs to focus on the deflection of the needle. However, since rigid needles are used in venipuncture and have a small range of motion, needle deflection can be ignored.

Compared to puncturing biological organs, research on venipunctures is relatively scarce, and the main reason is that venipuncture equipment requires dexterous working spaces, precise movements, and superior stabilities. Till date, there is no biomechanical model of venipuncture, and only a few studies on venipuncture processes have been reported. However, it has been demonstrated that variations in puncture force can be used to guide automated venipuncture. For

example, Satio et al. [22] performed a rabbit ear vein puncture under specific conditions and showed the generation of abrupt changes in the force curve. Li et al. [40] performed puncture experiments on a model and studied the force variations when the vessel and needle were misaligned. Kobayashi et al. [41] obtained the most straightforward conditions for stopping needle movement in the vein (insertion angle of 10-20° and velocity of 3 mm/s) by inserting the needle into the porcine jugular vein to obtain a puncture reaction force and assessing the change in force.

Therefore, we propose a robotic humanoid venipuncture method based on a biomechanical model to efficiently solve the venipuncture robot's ability to sense puncture status and position. This method mimics the human sensory and feedback control of the needle movements to guide and improve the performances of venipuncture robots. The model was verified by simulation, in vivo, and in vitro experiments, which indicated that the biomechanical model of venipuncture was universally applicable, and the humanoid venipuncture method based on the model was effective. The main contributions of this study are highlighted as follows: 1) a biomechanical model of venipuncture is established by analyzing the needle-tissue interactions, including elastic deformation, tissue cutting, and friction; and the model is validated in various conditions. 2) The robotic humanoid venipuncture method based on the model can percept the puncture state only by force signal with fewer hardware requirements. It is evaluated in vivo experiments by a self-developed six-degree-of freedom venipuncture robot.

The remainder of this paper is organized as follows. Section II analyzes the needle–tissue interactions during puncture and the developed biomechanical model. Section III presents the simulations and in vitro experiments of the venipuncture process and in vivo experiments of the humanoid puncture method based on the biomechanical model. Section IV summarizes the results of these experiments, and Section V contains a discussion and analysis of the experiments. Finally, Section VI presents a summary and conclusions of the study.

2 Venipuncture Method

2.1 Biomechanical Modeling of Venipuncture

Venipuncture can be divided into three stages with different forces. The puncture needle interacts with tissues and is subjected to elastic forces, cutting counterforces, and frictional forces mainly from tissue deformation, rupture, mutual compression, and friction. In addition, the force from the blood after entering the vessel may be negligible owing to the low venous blood pressure (about 1E-3 MPa) and small force area of the needle.

2.1.1 Elastic Force

The deformation phase causes elastic forces because of the viscoelasticity of soft tissues. Therefore, the generation of elastic forces between the puncture needle and soft tissues can be considered an elastic contact problem. Owing to the small diameter of the puncture needle relative to the size of the soft tissues, the surfaces of the two bodies are initially in contact at a single point, and a local stress concentration is generated at the contact area, which is nonconformal contact. When the contact area is tiny, it is possible to analyze only one infinitely large object subjected to a point load and ignore the other object. The elastic force F_E on the puncture needle and force F'_E on the tissues during elastic deformation generation constitute a pair of action and reaction forces, so F_E can be solved by analyzing F'_E; F'_E can be decomposed into a normal force $F'_{E,x}$ on the tissue and a tangential force $F'_{E,y}$. The tissue deformation in the depth direction is affected only by the normal force $F'_{E,x}$. Therefore, the Sneddon solution of the elastic contact problem [42] is used to solve for $F'_{E,x}$, which results in the elastic force F_E.

The puncture needle is in contact with the soft tissue at the point O' and the coordinate system $uO'\rho$ is established as shown in Fig. 2. The radius of the contact circle in the elastic half-space is a, and the distance between the surfaces $u = f(x) = f(\rho/a)$ and $f(0) = 0$ The boundary conditions are

$$\begin{cases} \sigma_{\rho u}(\rho, 0) = 0, \rho \le a \\ \sigma_{uu}(\rho, 0) = 0, \rho > a \end{cases} \tag{1}$$

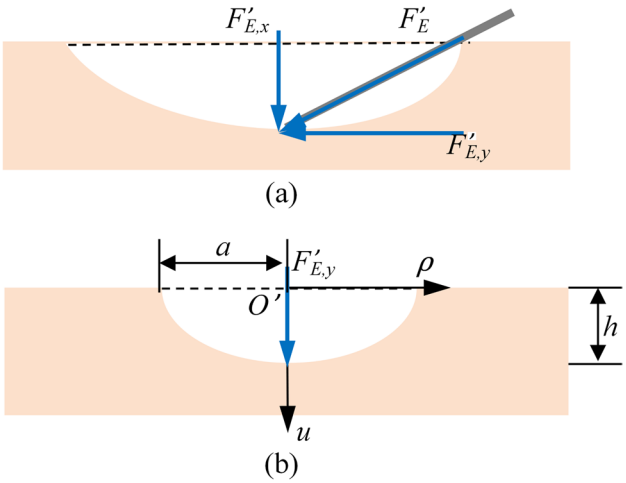

Fig. 2 Effects of elastic forces: (**a**) total elastic force and (**b**) Elastic force along the y-direction

where $\sigma_{\rho u}(\rho,0)$ is tangential stress, $\sigma_{uu}(\rho,0)$ is normal stress, and ρ is the distance from O' in axis ρ on the surface.

Under the normal force $F'_{E,x}$, the normal stress outside the contact radius is 0, and the tangential stress at the contact surface is 0. In the process of elastic deformation of the tissue, the stress and the maximum deformation are Eqs. 2 and 3,

$$\sigma_{uu}(\rho,0)=\frac{E}{ax\left(1-\upsilon^2\right)}\frac{d}{dx}\int_1^x\frac{t\chi(t)dt}{\sqrt{t^2-x^2}} \tag{2}$$

$$h=\int_0^1\frac{f'(x)dx}{\sqrt{1-x^2}} \tag{3}$$

$$\chi(t)=\frac{2}{\pi}\left\{\int_0^1\frac{f'(x)dx}{\sqrt{1-x^2}}-t\int_0^t\frac{f'(x)dx}{\sqrt{t^2-x^2}}\right\} \tag{4}$$

where E and υ are the equivalent elastic modulus and Poisson ratio of the tissue, respectively. Therefore, in the elastic half-space, $F'_{E,x}$ is given as

$$F'_{E,x}=\int_{-a}^{a}\int_0^{\pi}\sigma_{uu}(\rho,0)d\theta d\rho=\frac{4Ea}{1-\upsilon^2}\int_0^1\frac{x^2f'(x)dx}{\sqrt{1-x^2}} \tag{5}$$

where θ is the angular range of the elastic half-space, and $\theta\in[0,\pi]$. Since the puncture needle is in point contact with the tissue, the surface shape function of the needle tip can be simplified to $f(x)=ax\tan\beta$ (β is the bevel of the needle) and substituted into Eqs. 3 and 5 to obtain

$$h=\int_0^1\frac{f'(x)dx}{\sqrt{1-x^2}}=\frac{1}{2}\pi a\tan\alpha \tag{6}$$

$$F'_{E,x}=\frac{\pi Ea^2}{1-\upsilon^2}\tan\beta=\frac{4E\cot\beta}{\left(1-\upsilon^2\right)\pi}h^2 \tag{7}$$

Therefore, the elastic force is given by

$$F_E=\frac{F'_{E,x}}{\sin\alpha}=\frac{4E\cot\beta}{\left(1-\upsilon^2\right)\pi\sin\alpha}h^2 \tag{8}$$

where α is the needle insertion angle.

2.1.2 Cutting Counterforce

There are often many small cracks and defects in a given material. As the deformation increases, these cracks expand when the force exceeds a certain level, thereby leading to tissue destruction [43]. The puncture needle is subjected to a cutting counterforce, under which the crack size expands from a point to a circle of radius R (equal to the radius of the puncture needle). Thus the work done by the needle in producing a displacement of δl is equal to the energy δW_C required to produce the crack and strain energy δW_S inside the tissue, i.e.,

$$P\delta l=\delta W_C+\delta W_S \tag{9}$$

$$\delta W_C=J_{IC}(R,V)s\delta l \tag{10}$$

$$\delta W_S=\frac{1}{2}\pi GR^2\delta l \tag{11}$$

where s is the crack length that is constant when the puncture needle is determined. Owing to the viscoelasticity of biological tissues, the crack length can be considered as $s=2R$. $J_{IC}(R,V)$ is the first mode of fracture stiffness, which is related to the tissue properties and is proportional to the velocity when the puncture needle specifications are determined [33]; G is the shear modulus of the material, so the cutting reaction force is

$$F_C=2RJ_{IC}(R,V)+\frac{1}{2}\pi GR^2 \tag{12}$$

2.1.3 Frictional Force

Once the puncture needle enters the soft tissue, the surrounding soft tissue is deformed, which squeezes the needle and produces friction between the needle and tissue. The frictional forces are related to the material properties of the puncture needle and tissue, contact area, and needle insertion speed. It is caused by soft tissue adhesion and damping effects, so the mathematical model of the friction force during puncture can be constructed based on the LuGre model [44].

$$F_f=k_1F_N+k_2V \tag{13}$$

where k_1 and k_2 are the damping and sliding friction coefficients, respectively, and F_N is the positive pressure perpendicular to the axial direction of the piercing needle. In the friction process between the metal and hyperelastic material, the sliding friction coefficient k_2 decreases with an increase in velocity [45].

According to the Winkle foundation beam model [46],

$$F_N=kAb \tag{14}$$

where k is the base bed coefficient and settling volume $b=R$. The contact area between the puncture needle and tissue is $A=(2\pi Rl)/\sin\alpha$, l is the depth of needle entry and L is the distance of the upper wall of the vessel from the soft tissue surface. Thus, the frictional force is

$$F_f = \frac{2\pi R^2 k_1 kl}{\sin\alpha} + k_2 V \tag{15}$$

Hence, the biomechanical model during venipuncture is given by Eq. 16.

$$F = \begin{cases} \frac{4E\cot\beta}{(1-\upsilon^2)\pi\sin\alpha}h^2, \ \textit{Elastic deformation stage} \\ 2RJ_{IC}(R,\ V) + \frac{1}{2}\pi GR^2 \\ +\frac{2\pi R^2 k_1 kl}{\sin\alpha} + k_2 V, \ \textit{Cutting tissue stage} \\ \frac{2\pi R^2 k_1 kL}{\sin\alpha} + k_2 V, \ \textit{Entry into the vascular stage} \end{cases} \tag{16}$$

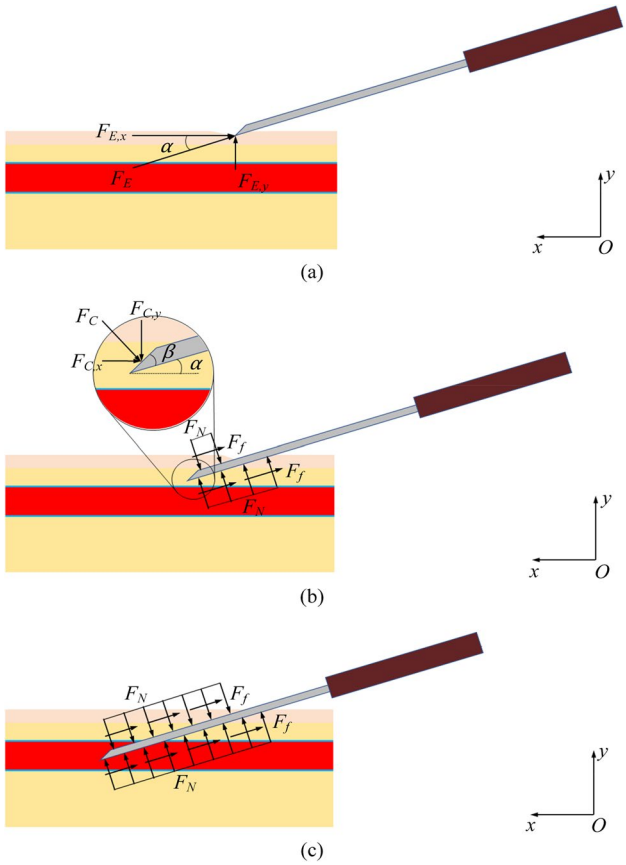

Fig. 3 Three stages of venipuncture: (**a**) elastic deformation, (**b**) tissue cutting, and (**c**) vascular entry stages

2.2 Humanoid Puncture Method Based on the Biomechanical Model

The biomechanical model of venipuncture is analyzed in Fig. 3. When the puncture needle and soft tissue contact and produce elastic deformation, there is an elastic force only between the needle and tissue, which is the elastic deformation or first stage of venipuncture. As the deformation increases, the force between the needle and tissue gradually increases until the tissue is destroyed. The needle continues to move while cutting tissue and is impeded by soft tissue so that cutting and frictional forces are generated, which is the second or tissue cutting stage of venipuncture. Here, the needle is subjected to cutting counterforces and frictional forces. When the puncture needle enters the upper wall of the vessel into the bloodstream, ignoring the effects of blood pressure, the cutting counterforce disappears, and the needle is subjected to tissue resistance and friction. This force produces a sudden drop in the axial direction along the needle, which is the third or vascular entry stage of venipuncture.

In manual venipuncture, the needle tip is considered to have entered the vessel when the medical staff senses sudden smoothness in the needle movements. According to the biomechanical venipuncture model, this feature's manifestation is caused by a sudden decrease in force. Therefore, the venipuncture robot can mimic the perception and feedback of the medical staff based on the biomechanical model to control the needle movements. As shown in Fig. 4, the robot collects data through high-resolution force sensors and sends the data to a host computer for processing and analysis. The robot is controlled to stop moving when the host computer judges that the needle has entered the vein according to the sudden decrease of force.

3 Experimental Setup

3.1 Design of Experimental Platform

The experiments in this work were all performed on the self-developed venipuncture robot (Figs. 5a and b). The robot requires a small working space during venipuncture but must have flexible motion, high accuracy, and rapid responses. The robot has a positioning arm and an end effector. It has six degrees of freedom with a decoupled position

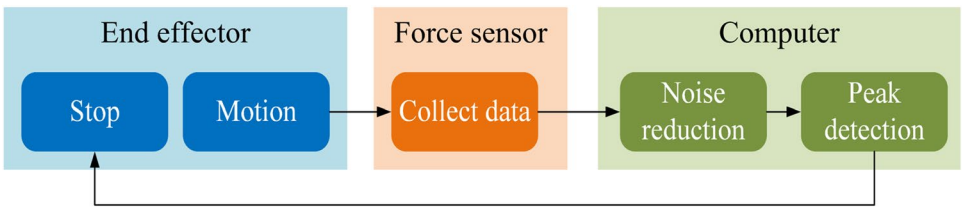

Fig. 4 Control flow of the puncture needle

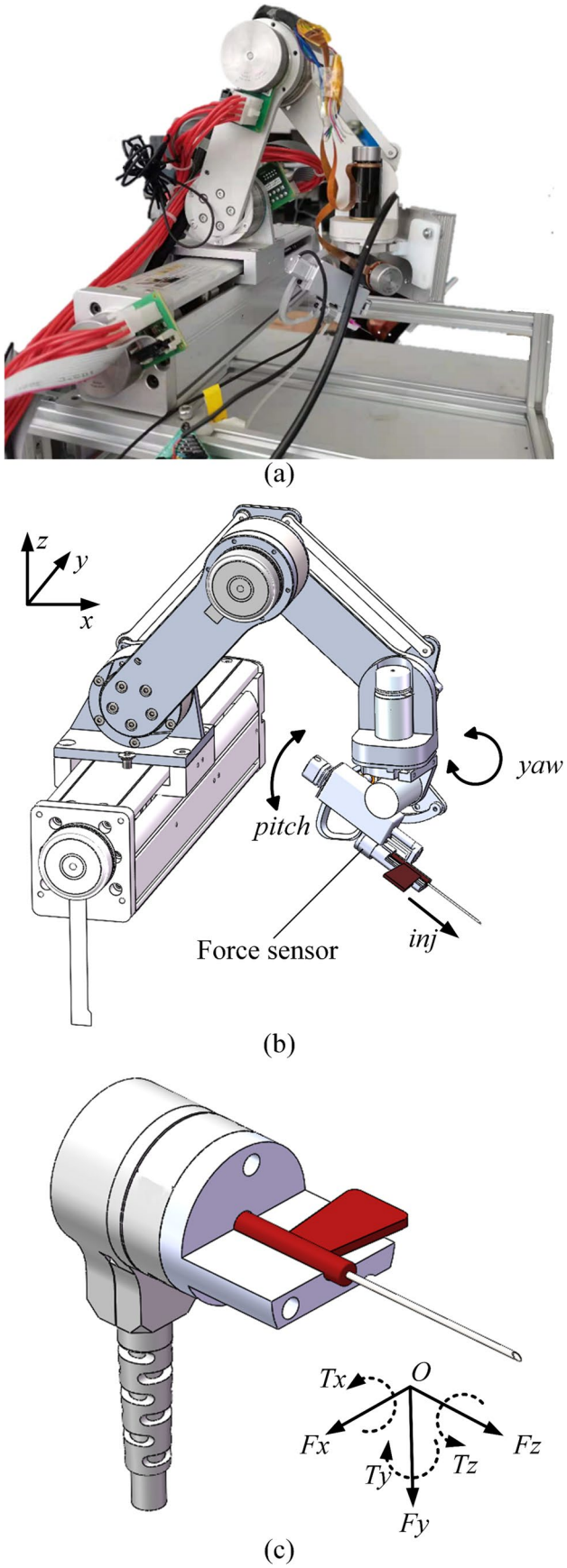

Fig. 5 (**a**) photograph of the experimental platform, (**b**) model of the experimental platform, and (**c**) installation of the force sensor and puncture needle

and attitude to improve motion accuracy and reduce control difficulty.

The positioning robot arm contains three degrees of freedom of movement in Cartesian space to realize the positioning of the end effector in a working space of 70mm × 80mm × 40mm and repeatable positioning accuracy of 0.006mm. The end effector has sufficient degrees of freedom to adjust the yaw and pitch angles (Figs. 6b and c), which can adjust the angular position of the needle relative to the vessel. The adjustment ranges are -45° to 45°and 0 to 30°, respectively, and the repeatable positioning accuracy is 0.06°. The feed mechanism enters and extracts the puncture needle with a miniature linear actuator (Inspire-Robots LASF16 series) with a stroke of 16mm and a movement accuracy of 0.03mm to realize high-precision movements over a small range.

A six-dimensional force sensor ATI-Nano17 (model SI-50-0.5, Fig. 5c) was mounted on the robot end-effector to measure small force changes during venipuncture. It was connected to a universal puncture needle (model 24G, Φ0.55mm × 19mm) to measure the force (acquisition frequency of 20 Hz) and process and analyze data through the host computer. The force sensor has high resolution and rapid response, and the range meets the measurement requirements. The ranges of *Fx* and *Fy* are 50N each, the range of *Fz* is 70N, and the resolution is1/80N.

3.2 Simulation of Puncture Process and In Vitro Experiments Based on Pork Phantom

This study simulated venipuncture in Ansys software under different conditions, and in vitro experiments were performed with a pork phantom. In the simulations, the puncture needle movement stopped when it reached the vessel's center. In contrast, each in vitro experiment was performed as a complete venous puncture (the needle entered the vessel for several seconds and was then withdrawn). The model used for the puncture process simulation contained four layers of tissues, skin, fat, muscle, and blood vessels, as shown in Fig. 7a. The model size was 10mm × 20mm × 15mm. The blood vessel with 3.5mm outer diameter and 3mm inner diameter was located in the fat layer. The parameters of the material of each layer were set in Table 1 [47, 48]. The puncture needle used was a 24G universal blood collection needle (Φ0.55mm × 19mm), and its material was structural steel. The tissues were set as fixed contact with each other, and the puncture needle was set for frictional contact with each layer of tissue, with a pressure of 1000Pa added to the vessel wall.

A venipuncture pork phantom was prepared under the human forearm anatomy model for in vitro experiments.

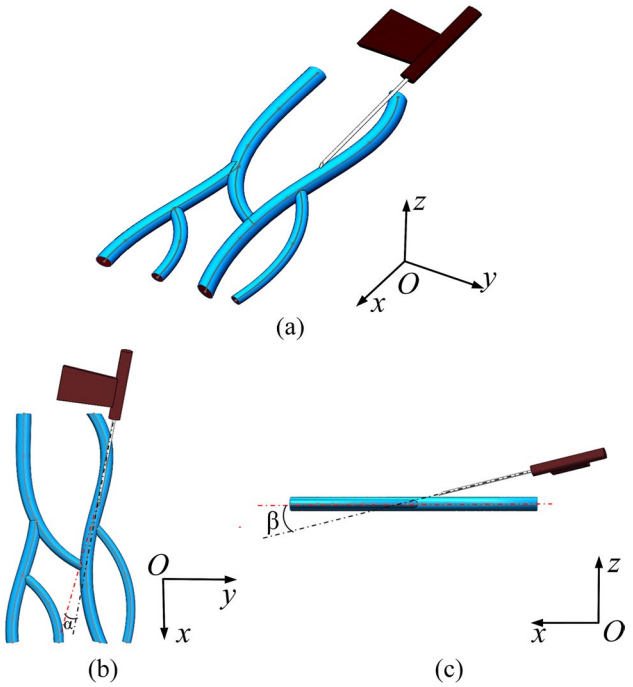

Fig. 6 (**a**) The three-dimensional relationship between needle and vein, (**b**) schematic diagram of yaw angle α, and (**c**) pitch angle β

Since pork has excellent mobility, the entire model is placed in a container to prevent excessive mobility of the phantom during venipuncture leading to failure. The bedding material, pork muscle, pork fat, and pigskin were placed in order from the bottom in a rectangular container. A rubber tube with a 3mm inner diameter and 4mm outer diameter was embedded in the pork fat to simulate a venous vessel, as shown in Fig. 7b.

Venipuncture was simulated at different needle deflection angles (0°, 45°, 90°, 135°, and 180°, as shown in Fig. 8). Then, experiments were simulated and conducted in vitro for different pitch angles (10°, 20°, and 30°) and needle insertion velocities (5mm/s, 10mm/s, 15mm/s, and 20mm/s) to explore the effectiveness of the biomechanical model and humanoid puncture method based on the model under different conditions.

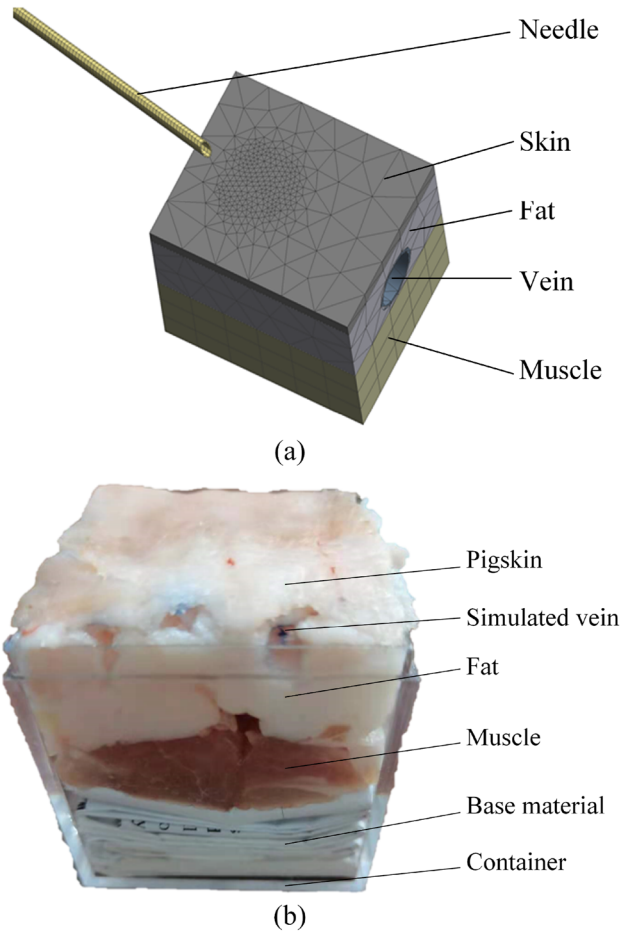

Fig. 7 (**a**) simulation model in Ansys, and (**b**) pork phantom used in the experiment

Table 1 The parameters of the mechanics of biological tissue

Yeoh Model			Mooney-Rivlin Model		
Tissue	Skin	Vessel	Tissue	Fat	Muscle
C10(MPa)	0.5	0.4	C10(MPa)	0.1	1
C20(MPa)	-0.06	-0.05	C01(MPa)	-0.04	-0.5
D1(MPa-1)	0.01	0.01	D1(MPa-1)	0.01	0.1
D2(MPa-1)	0.1	0.12	-	-	-

3.3 In Vivo Experiments Based on Rabbit Ear Vein

In vivo experiments were performed with the robotic system (Fig. 5c) on a rabbit's ear vein (Fig. 9). The humanoid puncture method based on the biomechanical model was applied, and the puncture site was selected manually according to the segmentation image of veins [49]. During robotic puncture, force data were collected and processed for analysis. The robot stopped moving when it determined that the puncture needle had entered the vessel. The puncture was deemed successful by observing the blood collected in the vacuum tube.

Two Chinese white rabbits (4kg weight) were used for the in vivo venipuncture experiments. The experimental protocols conformed to the ethical review guidelines for animal experiments at Harbin Institute of Technology, reduced the animals' pain to the maximum extent possible, and did not cause damage to the animals. The limbs and heads of the rabbits were fixed without anesthesia on a medical laboratory table using elastic bandages.

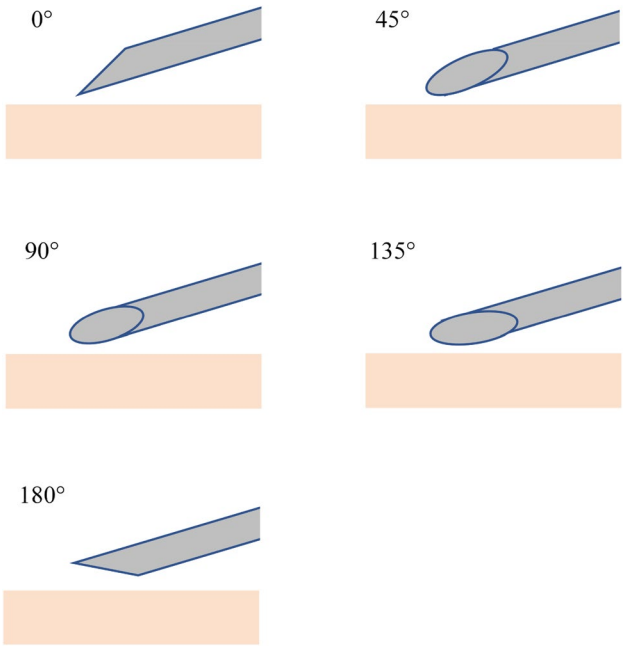

Fig. 8 Diagram showing deflection angles

Fig. 9 Rabbit ear vein used in the experiment

The rabbits' ears were fixed using medical elastic tape to expose the ear veins, which were about 1–2mm in diameter. Two punctures were performed on the rabbits' left and right ear veins in one day, and the rabbits were allowed to recover for one week before the next set of experiments, for a total of 25 experiments. The experimental parameters were chosen in the experiment to have a deflection angle of 0°, a pitch angle of 10°, and a needle velocities speed of 10mm/s.

4 Results

4.1 Simulation of Venipuncture and In Vitro Experiments Based on Pork Phantom

The puncture force is mainly distributed axially along the puncture needle, which is similar to that in the venipuncture simulation, as shown in the in vitro experiments in Figs. 10a and b. The force changes in the other directions are small and negligible compared with F_z. Meanwhile, three peaks, A, B, and C, were generated during the puncture simulations when puncturing the skin, fat, and blood vessel. Only one peak was observed in the puncture phantom when piercing the blood vessel. When the deflection angle, pitch angle, and needle speed were varied, the puncture forces had the same trends, increasing to a peak and then decreasing abruptly. The results of the in vitro experiments are similar to those of the puncture simulations. However, there is a strong regularity in the sudden drop of the puncture force in the simulated results. As shown in Table 2, the degree of sudden drop decreases

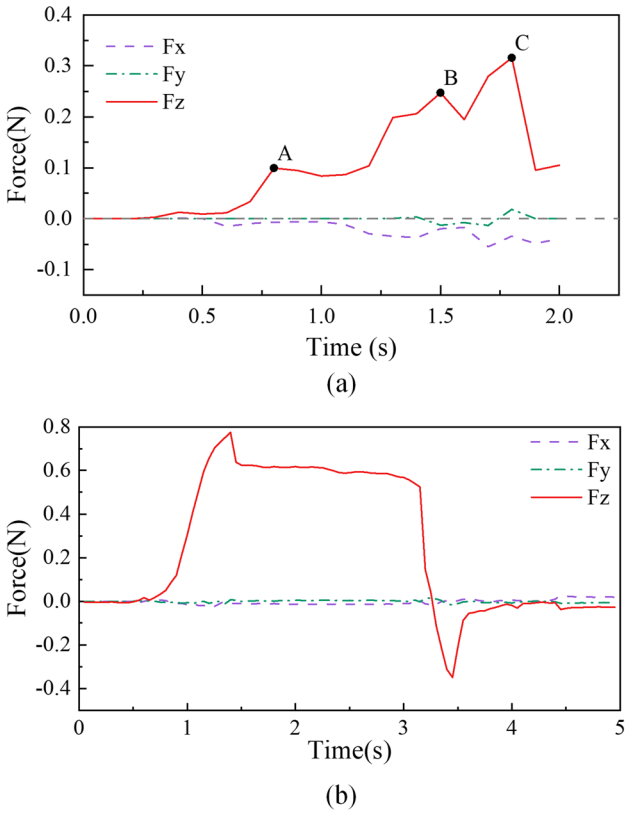

Fig. 10 Curves showing force changes in the simulations and in vitro experiments: (**a**) comparison of the three-dimensional forces in the puncture simulation, and (**b**) comparison of the three-dimensional forces in the in vitro experiments

Table 2 Peak puncture forces and vessel deformations under different puncture conditions

		Simulation			In vitro experiment	
		Peak force (N)	Percentage of sudden drop in force (%)	Vascular deformation (mm)	Peak force (N)	Percentage of sudden drop in force (%)
Deflection angle of needle[a]	0°	0.490	42.70	0.164	-	-
	45°	0.456	42.83	0.178	-	-
	90°	0.513	34.65	0.195	-	-
	135°	0.464	32.69	0.205	-	-
	180°	0.450	29.98	0.212	-	-
Pitch angle[b]	10°	0.696	28.83	0.112	0.780	44.87
	20°	0.607	33.72	0.135	0.761	44.34
	30°	0.490	42.70	0.164	0.749	29.49
Insertion speed[c]	5 mm/s	0.548	41.90	0.165	0.759	36.94
	10 mm/s	0.490	42.70	0.164	0.749	29.49
	15 mm/s	0.468	41.80	0.168	0.630	34.30
	20 mm/s	0.436	41.85	0.167	0.597	24.93

[a]Fixed pitch angle of 30° and needle insertion speed of 10 mm/s for puncture simulations at different deflection angles.

[b]Fixed deflection angle of 0° and needle insertion speed of 10 mm/s for puncture simulations and in vitro experiments at different pitch angles.

[c]Fixed deflection angle of 0° and pitch angle of 30° for puncture simulations and in vitro experiments at different needle insertion speeds.

with increasing deflection angle and increases with increasing pitch angle. The effects of needle insertion speed are not apparent. In contrast, in the in vitro experiments, there were no apparent regularities in the degrees of abrupt change, but all exceeded 28%.

The peak force changed with the deflection angle, pitch angle, and needle insertion speed during venipuncture, but the degrees of change differed between the venipuncture simulations and in vitro experiments. The peak force decreased with increasing pitch angle, which changed significantly for the venipuncture simulation but only to a small extent in the in vitro experiments (Fig. 11). In contrast, the peak force decreased with increasing needle insertion velocity in the in vitro experiments but changed to a lesser extent in the puncture simulations (Fig. 12). Meanwhile, the deflection angle had negligible effects on the peak force value (Fig. 13). In addition, the vessel deformations during puncture increased with increasing deflection and pitch angles and were less correlated with the needle insertion speed. When the velocity was increased by four times, the deformation increased by only 0.002 mm.

The tissue deformation and vessel deformation for a puncture simulation are shown in Fig. 14. The maximum deformation of the veins is the same as the maximum deformation of the tissues (containing fat, muscle, and blood vessels).

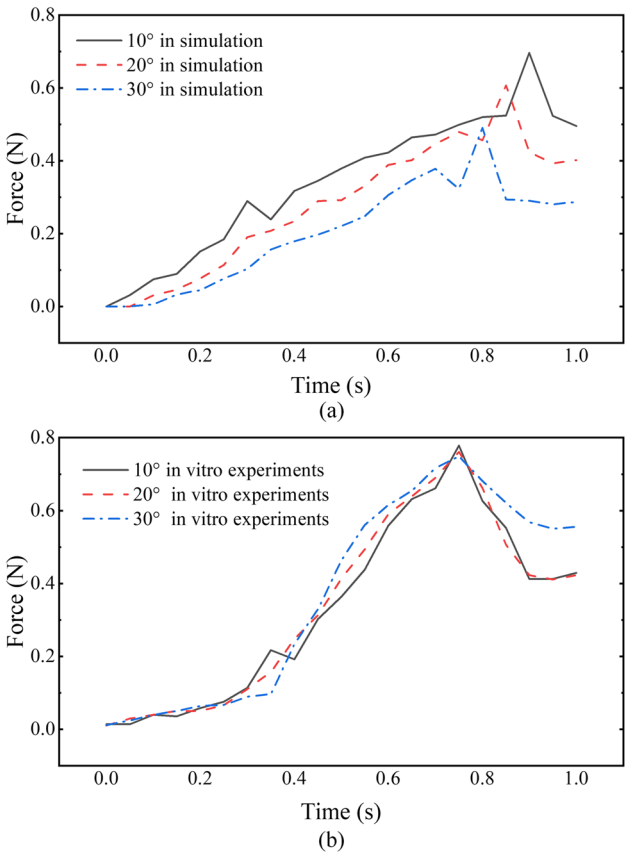

Fig. 11 Comparison of the forces for different pitch angles: (**a**) the forces in the puncture simulation, and (**b**) the forces in vitro experiments

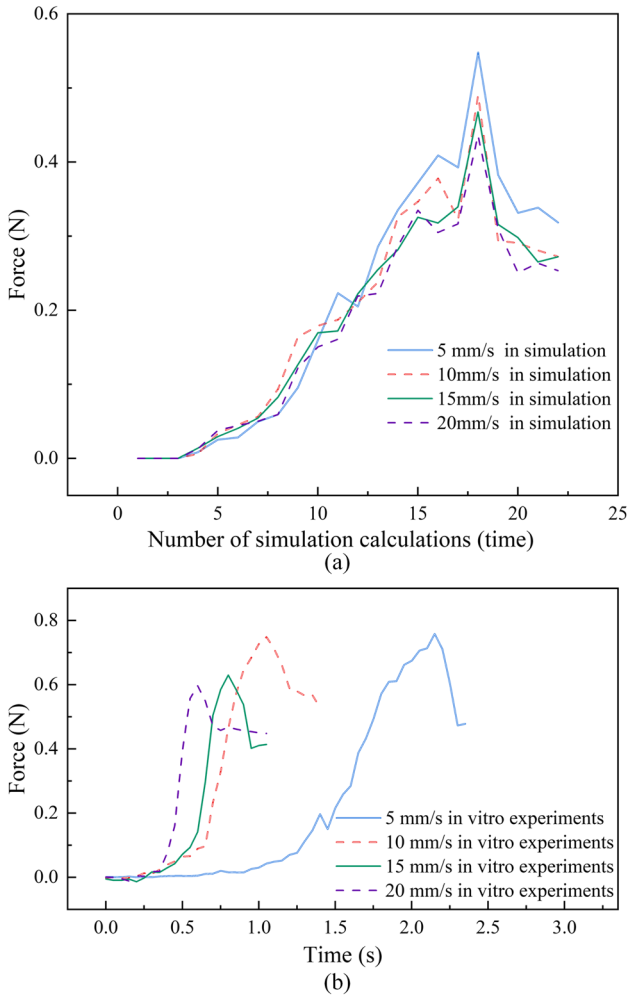

Fig. 12 Comparison of the forces for different needle insertion speeds: (**a**) the forces in the puncture simulation and (**b**) the forces in vitro experiments

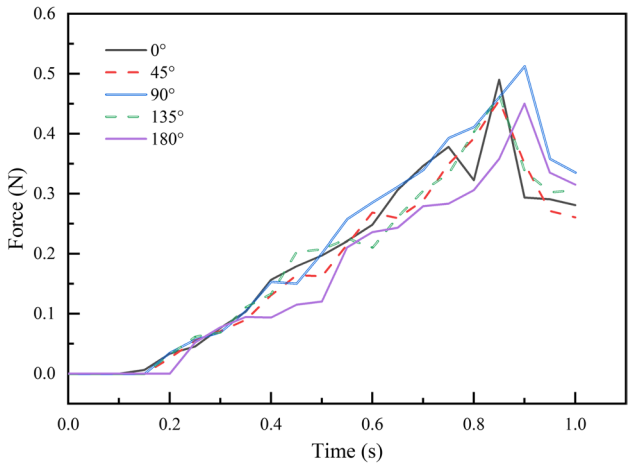

Fig. 13 Comparison of the forces in the puncture simulation for different deflection angles

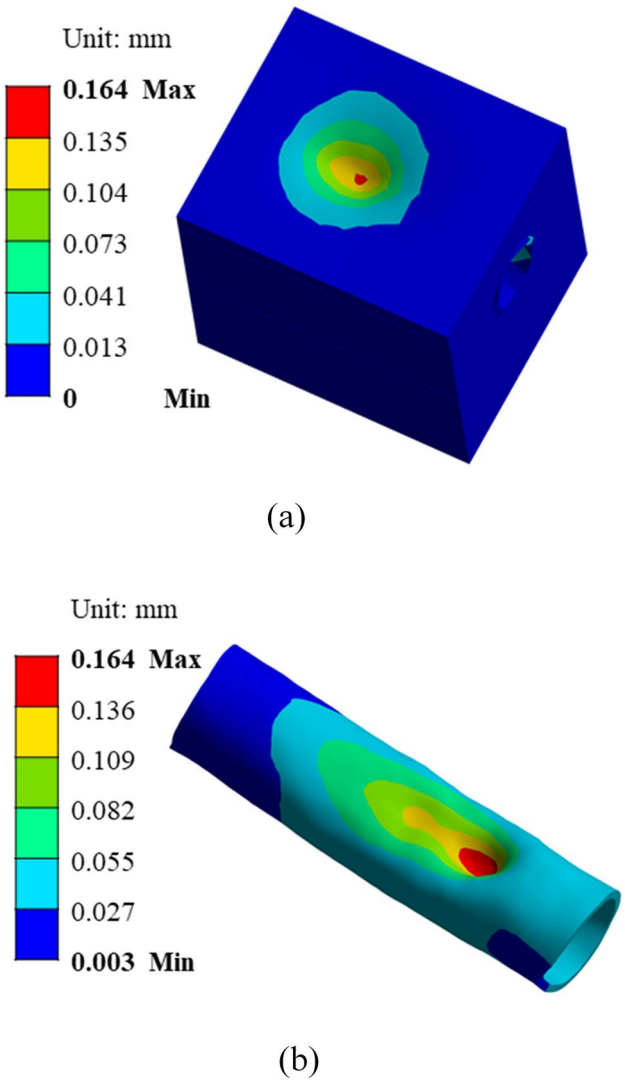

Fig. 14 (**a**) The deformation of tissue and (**b**) the deformation of the vein in a puncture simulation

4.2 In Vivo Experiments Based on Rabbit Ear Vein

The force data collected from in vivo experiments had the same trends as the simulated and in vitro experimental results. The puncture force started increasing when the needle tip touched the skin of the rabbit's ear and suddenly decreased before the robot stopped. A success rate of 88% was obtained for 22 out of 25 experiments, and almost reproducible results were obtained for all the successful experiments. The peak puncture force was 0.2326 ± 0.0452N, and the average decrease in puncture force was 64% when the abrupt change was produced. While conducting the experiments, the peak detection required an average time of 0.196s, and the robot responded with an average time of 0.162s. One of these results is depicted in Fig. 15, where the peak is seen at 3.699 s (point A), detected at 3.878 s (point B), and the robot stopped moving at 3.908 s (point C).

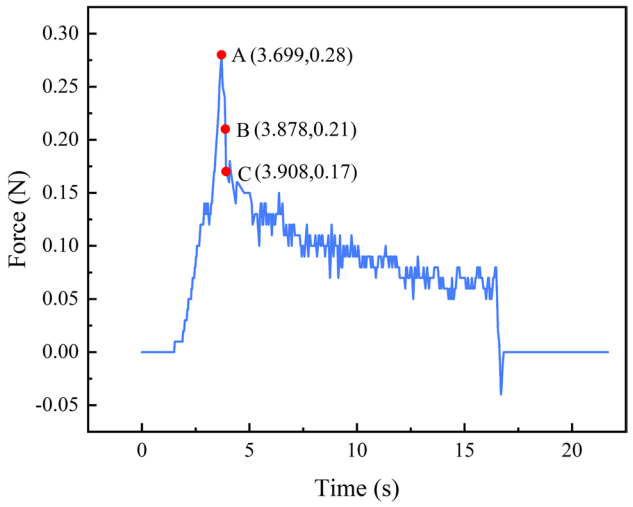

Fig. 15 Automated puncture experiments with rabbit ear veins

5 Discussion

This work proposed a robotic humanoid venipuncture method based on a biomechanical model to ensure that the robot can perceive the position of the puncture needle during venipuncture. Experiments were performed to show that the proposed method enables the robot to sense the needle state and position through force changes in automatic venipuncture. This is similar to imitating the actions of medical staff who control the needle movements based on perceptions. In cases where the puncture needle enters the tissue and cannot be seen, venipuncture failure caused by the needle not entering the vessel or piercing both ends of the vessel walls is avoided.

Compared with complicated surgical robots, venipuncture needles have a short journey and do not interact with rigid objects (bones) [7]. The working environment is relatively fixed and has higher stability. Of course, the process from skin contact to blood vessel entry of the venipuncture robot is no more than 3s, and the whole process requires a higher response speed. Therefore, surgical robots have higher requirements for accurate terminal control [8], while venipuncture robots have higher requirements for the response time of state perception. In this method, the interaction force between needle and tissue is used to perceive the puncture state, and the advantage is simple signal processing and quick robot response.

The interactions between needle and tissue based on manual venipuncture were analyzed, and a biomechanical model of venipuncture was proposed. The model guides the robot to imitate the actions and perceptions of the medical staff for venipuncture feedback. Unlike the biomechanical models for cutting organs, such as those of the bovine liver [34] and prostate [50], when the puncture needle enters the vessel, a sudden force change occurs in venipuncture. At the same time, the puncture force is almost constant because the needle-tissue contact area and the friction force remain constant [39]. This can be verified by the simulated results and in vitro and in vivo experiments.

Meanwhile, reproducible force results are obtained for successful venipuncture, regardless of the puncture conditions. The reason is that the cutting force between the needle and tissue disappears, and only the frictional force acts in the axial direction of the needle. Barnett et al. [33] predicted the puncture force in living tissues through a model and showed that an average of 61% of the force during insertion is from tissue cutting. Similarly, in vivo experimental results in this work show a sudden decrease of 64% in the puncture force, which coincides with the disappearance of the cutting force in the third stage of the venipuncture biomechanical model. Owing to the difference between the phantom and living biological tissues, the force decreased by 24% to 44% at successful puncture in simulation and in vitro phantom experiments. These results demonstrate the validity of perceiving the puncture state by force mutation.

The venipuncture biomechanical model proposed in this study divides the venipuncture process into three stages: elastic deformation, tissue cutting, and vascular entry. The model is validated by three relatively significant changes in the simulation results, as shown in Fig. 10a. There is fixed contact between the material layers in the venipuncture simulations, which differs from the interactions between actual biological tissues. Hence, no significant changes are observed when the puncture needle enters different material layers. The puncture force curves are relatively smooth in the in vivo and in vitro experiments, except for the abrupt changes in force after the puncture needles enter the vessels. The puncture needle produces a small abrupt change at small pitch angles and low needle insertion velocities when puncturing the skin layer. This result is similar to that observed in the experiments of Okuno et al. [51] on volunteers, but they did not observe this phenomenon with rabbit ear veins. One of the reasons for this is that the pitch angle used in the present experiment is different (10° was used in this work, whereas Okuno et al. used 15–30°). Another reason is the difference between rabbit ear tissue and human tissue, so Okuno et al. obtained different results for rabbits and volunteers.

According to the biomechanical model, the puncture force is elastic during the elastic deformation phase, related to the material properties, amount of deformation, and needle insertion angle. Since the material properties are constant, the maximum deformation is constant, and the elastic force is related only to the pitch angle. However, owing to the vessel's small size and minimal deformation, the elastic force differs less between simulations and experiments. In the tissue cutting phase, the puncture force consists of the cutting counterforce and frictional force. The cutting counterforce is independent of the pitch angle and is proportional to the needle insertion speed; the frictional force is related to the contact area and is inversely proportional to the needle insertion angle. As the insertion depth increases,

the contact surface between the tissue and the needle increases, thus increasing the friction. In addition, the sliding friction coefficient of the hyperelastic material decreases with an increase in the needle insertion velocity [45], which may explain why the increase in needle velocity causes a decrease in the puncture force in the simulations and in vitro experiments. This result is similar to the work of Casanova et al. [52] in brain tissue to study the relationship between force and velocity during puncture. However, the experimental findings of Boer et al. [1] are contrary to this result; this may seem possible because their experimental subjects were plastic phantoms, which have significantly different material properties than biological tissues.

This work selected a deflection angle of 0°, a pitch angle of 10°, and an insertion speed of 10 mm/s for the in vivo experiments. These parameter settings consider the need for smaller puncture forces to reduce pain during needle insertion [30] and minor vessel deformations to reduce the rate of puncture failure. When the deflection angle is 0°, the deformation of the tissue is minimized. An appropriate insertion speed and smaller pitch angle prevent damage to the vessels and other tissues due to needle overshoot.

Although some differences exist in the properties of the skin, fat layer, and other tissues between humans and animals, individual differences have been fully considered when using the biomechanical model. The model and experiments have shown that the forces have the same tendencies for successful venipuncture under different puncture conditions. Meanwhile, the venipuncture robot's puncture status is judged in real-time by online data acquisition, which is efficient and responsive [53, 54]. Therefore, it can be concluded that this work's biomechanical model and humanoid venipuncture method still apply to humans.

In several failed in vivo experiments, the puncture needles entered the tissue but did not extract blood. The main reason was that the vessels moved and rolled under the applied forces during venipuncture, thus preventing the needle from entering the vessels. The peak forces could not be detected in such cases and increased before the robot stopped moving.

6 Conclusion

The robotic humanoid venipuncture method based on a developed biomechanical model ensures that the robot can simulate the perception and feedback actions of medical staff during manual venipuncture to control the movements of the needle. By analyzing the venipuncture, the process was divided into three stages (elastic deformation stage, cutting tissue stage, and entry into the vascular stage). The biomechanical model was constructed by discussing the interaction forces between the needle and the tissue in each process. The venipuncture simulations performed in Ansys and in vitro experiments are consistent with the model, verifying the validity. At the same time, the peak puncture force increases with increasing pitch angle and decreasing needle insertion speed and is less affected by the deflection angle. However, similar trends for changes in the puncture forces were found despite the different conditions, with a sudden drop of more than 20% in the puncture force when the vein was punctured. This is similar to the perception and feedback mechanisms in manual venipuncture. In in vivo experiments, automated puncture experiments of rabbit ear veins with a success rate of approximately 90% showed the utility of the robotic humanoid venipuncture method for effectively controlling the entry of the needle into the vessel. These results suggest that the proposed method is practical and helpful for improving the performances of venipuncture robots.

There are still some limitations. On the one hand, vessel deformations, movements, and rolling due to forces during venipuncture are not considered, which also makes the failed venipuncture. On the other hand, the model is not quantified and focuses on the sudden drop, not specific values. The future work mainly focuses on improving the biomechanical model considering the effect of tissue deformation on venipuncture. Also, a predictive model based on the quantified biomechanical model and deep learning will be constructed to feed forward the state of venipuncture further to improve the success rate of the venipuncture robot.

Author Contributions Tianbao He and Li Jiang conceived and designed the study. Tianbao He and Hansong Liu performed the experiments. Tianbao He wrote the paper. Tianbao He, Li Jiang, and Chuangqiang Guo reviewed and edited the manuscript. All authors read and approved the manuscript.

Funding This work was supported by the National Natural Science Foundation of China (U1813209), Self-Planned Task (NO. SKLRS202112B) of State Key Laboratory of Robotics and System (HIT).

Code or Data Availability Not applicable.

Declarations

Conflicts of Interest We declare that we have no financial and personal relationships with other people or organizations that can inappropriately influence our work. There is no professional or other personal interest of any nature or kind in any product, service, or company that could be construed as influencing the position presented in or the review of the manuscript entitled.

Ethics Approval This study did not cause harm to the subjects, and the subjects were well fed and cared for. We consulted extensively with the IRB that our study did not need ethical approval.

Consent to Participate Not applicable.

Consent for Publication Not applicable.

References

1. De Boer, T., Steinbuch, M., Neerken, S., Kharin, A.: Laboratory study on needle–tissue interaction: towards the development of an

instrument for automatic venipuncture. J. Mech. Med. Biol. 07, 325–335 (2007). https://doi.org/10.1142/S0219519407002297
2. Zeng, S., Yan, X.: Effect of compositive nursing measures on pedi-atric infusion compliance and comfort. Chin. J. Med. Guide. **19**, 88–90 (2017)
3. Douissard, J., Hagen, M.E., Morel, P.: The da Vinci surgical system. In: Domene, C.E., Kim, K.C., Vilallonga Puy, R., Volpe, P. (eds.) Bariatric robotic surgery: a comprehensive guide, pp. 13–27. Springer International Publishing, Cham (2019)
4. Zhang, W., Zhang, Y., Liu, Y.: Design and control of a bionic needle puncture robot. The International Journal of Medical Robotics and Computer Assisted. Surgery. **17**, e2200 (2021). https://doi.org/10.1002/rcs.2200
5. He, T., Guo, C., Ren, H., Jiang, L.: Research progress of venipuncture robot. J. Mech. Eng. **57**, 1–10 (2021)
6. Qi, W., Su, H.: A cybertwin based multimodal network for ECG patterns monitoring using deep learning. IEEE Trans. Industr. Inform. **1–1** (2022). https://doi.org/10.1109/TII.2022.3159583
7. Su, H., Qi, W., Chen, J., Zhang, D.: Fuzzy approximation-based task-space control of robot manipulators with remote center of motion constraint. IEEE Trans. Fuzzy Syst. **1–1** (2022). https://doi.org/10.1109/TFUZZ.2022.3157075
8. Su, H., Hu, Y., Karimi, H.R., Knoll, A., Ferrigno, G., De Momi, E.: Improved recurrent neural network-based manipulator control with remote center of motion constraints: Experimental results. Neural Netw. **131**, 291–299 (2020). https://doi.org/10.1016/j.neunet.2020.07.033
9. Hu, Y., Su, H., Chen, G., Ferrigno, G., De Momi, E., Knoll, A.: hierarchical optimization control of redundant manipulator for robot-assisted minimally invasive surgery. In: 2020 IEEE/RSJ International Conference on Intelligent Robots and Systems (IROS). pp. 2929–2934 (2020)
10. Hu, Y., Li, J., Chen, Y., Wang, Q., Chi, C., Zhang, H., Gao, Q., Lan, Y., Li, Z., Mu, Z., Sun, Z., Knoll, A.: Design and control of a highly redundant rigid-flexible coupling robot to assist the COVID-19 oropharyngeal-swab sampling. IEEE Robot. Autom. Lett. **7**, 1856–1863 (2022). https://doi.org/10.1109/LRA.2021.3062336
11. Qiao, Z., Li, Y., Wu, Z., Kou, J.: Automatic Puncture System Based on NIR Image and Ultrasonic Image. MATEC Web Conf. **108**, 15002 (2017). https://doi.org/10.1051/matecconf/201710815002
12. Balter, M.L., Chen, A.I., Maguire, T.J., Yarmush, M.L.: The system design and evaluation of a 7-DOF image-guided venipuncture robot. IEEE Trans. Robot. **31**, 1044–1053 (2015). https://doi.org/10.1109/TRO.2015.2452776
13. Harris, R.J., Grove, C., Mygatt, J.B.: Autonomous intravenous needle
14. Curtis, S.J., Craig, W.R., Logue, E., Vandermeer, B., Hanson, A., Klassen, T.: Ultrasound or near-infrared vascular imaging to guide peripheral intravenous catheterization in children: a pragmatic randomized controlled trial. CMAJ. **187**, 563–570 (2015). https://doi.org/10.1503/cmaj.141012
15. Dong, J.: Design and experiment of the prototype of venous blood drawing robot, https://kns.cnki.net/KCMS/detail/detail.aspx?dbcode=CMFD&dbname=CMFD202001&filename=1019649245.nh&v=, (2019)
16. Perry, T.: Profile: Veebot [Resources_Start-ups]. IEEE Spectr. **50**, 23–23 (2013). https://doi.org/10.1109/MSPEC.2013.6565554
17. Mwikirize, C., Nosher, J.L., Hacihaliloglu, I.: Convolution neural networks for real-time needle detection and localization in 2D ultrasound. Int J CARS. 13, 647–657 (2018). 10/gdkb74
18. Cheng, Z., Davies, B.L., Caldwell, D.G., Mattos, L.S.: A venipuncture detection system for robot-assisted intravenous catheterization. In: 2016 6th IEEE International Conference on Biomedical Robotics and Biomechatronics (BioRob). pp. 80–86. IEEE, Singapore, Singapore (2016)
19. Kim, A., Kim, Park, C.: Lock-in amplifier-based impedance detection of tissue type using a monopolar injection needle. Sensors. **19**, 4614 (2019). https://doi.org/10.3390/s19214614
20. Hyink, S., Whittemore, J.C., Mitchell, A., Reed, A.: Diagnostic accuracy of tissue impedance measurement interpretation for correct veress needle placement in feline cadavers: tissue impedance measurement interpretation for veress needle placement in cats. Vet. Surg. **42**, 623–628 (2013). https://doi.org/10.1111/j.1532-950X.2013.01098.x
21. Abbasi, M.A., Kim, H., Chinnadayyala, S.R., Park, K.D., Cho, S.: Real-time impedance detection of intra-articular space in a porcine model using a monopolar injection needle. Sensors. **20**, 4625 (2020). https://doi.org/10.3390/s20164625
22. Saito, H., Mitsubayashi, K., Togawa, T.: Detection of needle puncture to blood vessel by using electric conductivity of blood for automatic blood sampling. Sensors Actuators A Phys. **125**, 446–450 (2006). https://doi.org/10.1016/j.sna.2005.06.012
23. Al-Harosh, M.B., Shchukin, S.I.: Peripheral vein detection using electrical impedance method. **5** (2017)
24. AL-Harosh, M.B., Shchukin, S.I.: Numerical modeling of the electrical impedance method of peripheral veins localization. In: Jaffray, D.A. (ed.) World Congress on Medical Physics and Biomedical Engineering, June 7-12, 2015, Toronto, Canada, pp. 1683–1686. Springer International Publishing, Cham (2015)
25. Fontana, M., Fabio, S., Marcheschi, S., Bergamasco, M.: Haptic Hand Exoskeleton for Precision Grasp Simulation. Journal of Mechanisms and Robotics. 5, 041014 (2013). 10/gkgb2t
26. Wyke, M.: The effect of brain lesions in the performance of an arm-hand precision task. Neuropsychologia. 6, 125–134 (1968). 10/b9njsc
27. Su, H., Qi, W., Hu, Y., Karimi, H.R., Ferrigno, G., Momi, E.D.: An incremental learning framework for human-like redundancy optimization of anthropomorphic manipulators. IEEE Trans. Industr. Inform. **18**, 1864–1872 (2022). https://doi.org/10.1109/TII.2020.3036693
28. Su, H., Zhang, J., Fu, J., Ovur, S.E., Qi, W., Li, G., Hu, Y., Li, Z.: Sensor fusion-based anthropomorphic control of under-actuated bionic hand in dynamic environment. In: 2021 IEEE/RSJ International Conference on Intelligent Robots and Systems (IROS). pp. 2722–2727 (2021)
29. Nagchaudhuri, A., Garg, D.P.: Adaptive control and impedance control for dual robotic arms manipulating a common heavy load. In: 2001 IEEE/ASME International Conference on Advanced Intelligent Mechatronics. Proceedings (Cat. No.01TH8556). pp. 683–688. IEEE, Como, Italy (2001)
30. Cortesão, R., Dominici, M.: Robot force control on a beating heart. IEEE/ASME Transactions on Mechatronics. 22, 1736–1743 (2017). 10/gbtjmt
31. Osa, T., Sugita, N., Mitsuishi, M.: Online trajectory planning and force control for automation of surgical tasks. IEEE Transactions on Automation Science and Engineering. 15, 675–691 (2018). 10/gdcphx
32. Jiang, S., Li, P., Yu, Y., Liu, J., Yang, Z.: Experimental study of needle–tissue interaction forces: Effect of needle geometries, insertion methods and tissue characteristics. Journal of Biomechanics. 47, 3344–3353 (2014). 10/f6m2jm
33. Barnett, A.C., Lee, Y.-S., Moore, J.Z.: Fracture mechanics model of needle cutting tissue. J. Manuf. Sci. Eng. **138** (2015). https://doi.org/10.1115/1.4030374
34. Okamura, A.M., Simone, C., O'Leary, M.D.: Force modeling for needle insertion into soft tissue. IEEE Trans. Biomed. Eng. **51**, 1707–1716 (2004). https://doi.org/10.1109/TBME.2004.831542
35. Su, H., Fischer, G.S.: A 3-axis optical force/torque sensor for prostate needle placement in Magnetic resonance imaging environments. In: 2009 IEEE International Conference on Technologies

for Practical Robot Applications. pp. 5–9. IEEE, Woburn, MA, USA (2009)
36. Su, Z.: Force modeling for needle insertion into soft tissue and measurement of needle deflection
37. Fukushima, Y., Naemura, K.: Estimation of the friction force during the needle insertion using the disturbance observer and the recursive least square. Robomech J. 1, 14 (2014). 10/gn9qzm
38. Gordon, A., Kim, I., Barnett, A.C., Moore, J.Z.: Needle insertion force model for haptic simulation. In: Volume 2: Materials; biomanufacturing; properties, applications and systems; sustainable manufacturing. p. V002T03A003. American Society of Mechanical Engineers, Charlotte, North Carolina, USA (2015)
39. Datla, N.V., Konh, B., Honarvar, M., Podder, T.K., Dicker, A.P., Yu, Y., Hutapea, P.: A model to predict deflection of bevel-tipped active needle advancing in soft tissue. Med. Eng. Phys. **36**, 285–293 (2014). https://doi.org/10.1016/j.medengphy.2013.11.006
40. Li, Z., Li, M., Wei, J., Su, B., Pan, C., Kuang, S., Zhou, L.: A robotic system for investigation on mis-alignment force of needle and vein needle insertion into blood vessel. In: 2017 2nd Asia-Pacific Conference on Intelligent Robot Systems (ACIRS). pp. 280–283. IEEE, Wuhan, China (2017)
41. Kobayashi, Y., Hamano, R., Watanabe, H., Hong, J., Toyoda, K., Hashizume, M., Fujie, M.G.: Use of puncture force measurement to investigate the conditions of blood vessel needle insertion. Med. Eng. Phys. **35**, 684–689 (2013). https://doi.org/10.1016/j.medengphy.2012.12.003
42. Sneddon, I.N.: The relation between load and penetration in the axisymmetric boussinesq problem for a punch of arbitrary profile. International Journal of Engineering Science. 3, 47–57 (1965). 10/c445s9
43. Han, H.: Research on the friction and cutting model of bev-el-tip flexible needle insertion, https://kns.cnki.net/KCMS/detail/detail.aspx?dbcode=CMFD&dbname=CMFD201401&filename=1013036480.nh&v=, (2012)
44. Asadian, A., Kermani, M.R., Patel, R.V.: A compact dynamic force model for needle-tissue interaction. In: 2010 Annual International Conference of the IEEE Engineering in Medicine and Biology. pp. 2292–2295. IEEE. Buenos Aires. (2010)
45. Lv, R., Li, T., Huang, X.: Study on tribological behavior of NBR under variable velocity. China Synthetic Rubber Industry. **101–103** (2002)
46. Yankelevsky, D.Z., Eisenberger, M., Adin, M.A.: Analysis of beams on nonlinear winkler foundation. Computers & Structures. 31, 287–292 (1989). 10/bn49np
47. Yeoh, O.H.: Some forms of the strain energy function for rubber. Rubber Chem. Technol. **66**, 754–771 (1993) 10/dmrtw3
48. Ren, H.: Research on perception and control of full-automatic venipuncture robot, https://kns.cnki.net/KCMS/detail/detail.aspx?dbcode=CMFD&dbname=CMFD202101&filename=1020400374.nh&v=, (2020)
49. He, T., Guo, C., Jiang, L., Liu, H.: Automatic venous segmentation in venipuncture robot using deep learning. In: 2021 IEEE International Conference on Real-time Computing and Robotics (RCAR). pp. 614–619 (2021)
50. Kobayashi, Y., Sato, T., Fujie, M.G.: Modeling of friction force based on relative velocity between liver tissue and needle for needle insertion simulation. In: 2009 Annual International Conference of the IEEE Engineering in Medicine and Biology Society. pp. 5274–5278. IEEE, Minneapolis, MN (2009)
51. Okuno, D., Togawa, T., Saito, H., Tsuchiya, K.: Development of an automatic blood sampling system: control of the puncturing needle by measuring forces. In: Proceedings of the 20th Annual International Conference of the IEEE Engineering in Medicine and Biology Society. Vol.20 Biomedical Engineering Towards the Year 2000 and Beyond (Cat. No.98CH36286). pp. 1811–1812. IEEE, Hong Kong, China (1998)
52. Casanova, F., Carney, P.R., Sarntinoranont, M.: In vivo evaluation of needle force and friction stress during insertion at varying insertion speed into the brain. J. Neurosci. Methods. **237**, 79–89 (2014). https://doi.org/10.1016/j.jneumeth.2014.08.012
53. Lee, J., Jeon, W., Lee, B., Pineau, J., Kim, K.-E.: OptiDICE: offline policy optimization via stationary distribution correction estimation. In: Proceedings of the 38th International Conference on Machine Learning. pp. 6120–6130. PMLR (2021)
54. Meng, B., Wang, Y., Mao, J., Liu, J., Xu, G., Dai, J.: Using SoC online correction method based on parameter identification to optimize the operation range of NI-MH battery for electric boat. Energies. **11**, 586 (2018). https://doi.org/10.3390/en11030586

Tianbao He received the B.S. degree in Mechanical Engineering from Harbin Institute of Technology, Harbin, China, in 2018. He is currently pursuing the Ph.D. degree with the State Key Laboratory of Robotics and System, Harbin Institute of Technology. His research interests include venous perception and autonomous decision-making for the venipuncture robot.

Chuangqiang Guo received the B.S. and M.S. degrees from the Harbin University of Science and Technology, Harbin, China, in 2005 and 2008, respectively, and the Ph.D.degree from Harbin Institute of Technology (HIT), Harbin, China, in 2012, all in mechanical engineering. He is currently an Associate Research Fellow with the State Key Laboratory of Robotics and Systems, HIT. His research interests include the design and control technologies of ac motor drive and robotic systems.

Hansong Liu received the B.S. degree in Automation from Northeastern University, Shenyang, China, in 2020. He is currently pursuing the Master's degree with the State Key Laboratory of Robotics and System, Harbin Institute of Technology. His research interests include the design of sensing and control systems for the venipuncture robot.

Li Jiang received the B.S. degree in optical instrumentation from Tsinghua University, Beijing, China, in 1993, and the Ph.D. degree in mechanical engineering from the Harbin Institute of Technology, Harbin, China, in 2001. He is currently a Professor with the State Key Laboratory of Robotics and System, Harbin Institute of Technology. His research interests include the robotic hand, prostheses, medical robot, sensors and control algorithms.